

High-order geometric integrators for representation-free Ehrenfest dynamics

Seonghoon Choi^{a)} and Jiří Vaníček^{b)}

Laboratory of Theoretical Physical Chemistry, Institut des Sciences et Ingénierie Chimiques, Ecole Polytechnique Fédérale de Lausanne (EPFL), CH-1015, Lausanne, Switzerland

(Dated: 7 September 2021)

Ehrenfest dynamics is a useful approximation for *ab initio* mixed quantum-classical molecular dynamics that can treat electronically nonadiabatic effects. Although a severe approximation to the exact solution of the molecular time-dependent Schrödinger equation, Ehrenfest dynamics is symplectic, time-reversible, and conserves exactly the total molecular energy as well as the norm of the electronic wavefunction. Here, we surpass apparent complications due to the coupling of classical nuclear and quantum electronic motions and present efficient geometric integrators for “representation-free” Ehrenfest dynamics, which do not rely on a diabatic or adiabatic representation of electronic states and are of arbitrary even orders of accuracy in the time step. These numerical integrators, obtained by symmetrically composing the second-order splitting method and exactly solving the kinetic and potential propagation steps, are norm-conserving, symplectic, and time-reversible regardless of the time step used. Using a nonadiabatic simulation in the region of a conical intersection as an example, we demonstrate that these integrators preserve the geometric properties exactly and, if highly accurate solutions are desired, can be even more efficient than the most popular non-geometric integrators.

^{a)}Electronic mail: seonghoon.choi@epfl.ch

^{b)}Electronic mail: jiri.vanicek@epfl.ch

I. INTRODUCTION

Mixed quantum-classical methods, such as the surface hopping,^{1–5} mean-field Ehrenfest dynamics,^{6–15} and methods based on the mixed quantum-classical Liouville equation^{16–18} or the Meyer–Miller–Stock–Thoss mapping Hamiltonian,^{19–25} remedy one of the shortcomings of classical molecular dynamics: its inability to describe electronically nonadiabatic processes^{26–28} involving significantly coupled^{29–31} states. Although a severe approximation to the exact quantum solution,^{8,32,33} Ehrenfest dynamics can provide a useful first picture of nonadiabatic dynamics in some, especially strongly coupled systems. Indeed, Ehrenfest dynamics was successfully used to describe electron transfer,^{34–38} nonadiabatic processes at metal surfaces,^{39–42} and photochemical processes.^{43–45} The mean-field theory was also employed to simplify the evaluation of the memory kernel in the generalized master equation formalism.⁴⁶ In addition, Ehrenfest dynamics provides a starting point for various refined methods. For example, a multi-trajectory, locally mean-field generalization of Ehrenfest dynamics was used to evaluate vibronic spectra⁴⁷ and, when combined with the semiclassical initial value representation, can describe even wavepacket splitting.⁴⁸ A further generalization, the multiconfigurational Ehrenfest method,^{49–51} includes correlations between Ehrenfest trajectories. In what follows, we shall only consider the basic, mean-field Ehrenfest method, whose validity conditions were formulated by Bornemann *et al.*⁵²

The coupling between nuclear and electronic dynamics complicates the numerical integration in Ehrenfest dynamics. The widely-used two and three time step methods^{11–13,53,54} improve the efficiency by using different integration time steps that account for the different time scales of nuclear and electronic motions (see Appendix A). However, such integration schemes violate the geometric properties of the exact solution: the simpler, two time step method is irreversible and neither method is symplectic (see Fig. 6 in Appendix A). Almost every geometric property^{55–57} can, however, be preserved exactly by employing the symplectic integrators⁵⁸ based on the splitting method.^{59,60} This splitting method is widely applicable—so long as the Hamiltonian can be decomposed into exactly solvable parts—and was employed to obtain symplectic integrators in many well-known applications, including molecular quantum⁶¹ and classical⁶² dynamics, Schrödinger–Liouville–Ehrenfest dynamics,⁶³ and the Meyer–Miller–Stock–Thoss mapping approach.^{64–66} In particular, because the Ehrenfest method in either the adiabatic or diabatic representation can be formu-

lated as a special case of the mapping method,^{19,67} the integrators developed for one of these two methods should also be applicable to the other. Motivated by on-the-fly *ab initio* applications that employ increasingly practical real-time time-dependent electronic structure methods,^{68,69} here we present integrators that—in contrast to the integrators^{64–66} formulated in the mapping approach—do not rely on any particular representation of electronic states and thus avoid the expensive construction of a truncated diabatic or adiabatic electronic basis.

Typically, to reach the same accuracy, geometric integrators need greater computational effort than their non-geometric counterpart.^{55,56} Yet, the efficiency of geometric integrators can be improved significantly by employing various composition methods.^{55,56,70–74} Thus obtained integrators of high orders of convergence in the time step offer the best of both worlds: they are efficient while conserving the relevant geometric structure exactly.⁵⁶

After showing analytically, in Sec. II, that the high-order geometric integrators preserve almost all of the geometric properties of Ehrenfest dynamics, in Sec. III, we numerically demonstrate the efficiency and geometric properties of these integrators on a four-dimensional extension^{75–77} of the Shin–Metiu model.^{78,79} In this system, the first and second excited adiabatic states are coupled significantly due to a conical intersection. Section IV concludes the paper.

II. THEORY

A. Time-dependent Hartree approximation for the molecular wavefunction

Quantum evolution of a molecule is governed by the time-dependent Schrödinger equation (TDSE)

$$i\hbar \frac{d}{dt} \Psi_t = \mathcal{H} \Psi_t, \quad (1)$$

where Ψ_t denotes the molecular state at time t and \mathcal{H} is the molecular Hamiltonian. In general, we will denote operators acting on both nuclei and electrons by a calligraphic font, whereas the operators acting either only on nuclei or only on electrons will have a hat. The molecular Hamiltonian is equal to the sum

$$\mathcal{H} = \hat{T}_{\text{nu}} + \hat{T}_{\text{el}} + \mathcal{V} \quad (2)$$

of the nuclear kinetic energy operator

$$\hat{T}_{\text{nu}} = \frac{1}{2} \hat{P}^T \cdot M^{-1} \cdot \hat{P}, \quad (3)$$

electronic kinetic energy operator

$$\hat{T}_{\text{el}} = \frac{1}{2} \hat{p}^T \cdot m^{-1} \cdot \hat{p}, \quad (4)$$

and potential energy operator $\mathcal{V}(\hat{q}, \hat{Q})$. We assume that the nuclear position Q and momentum P are D -dimensional vectors, whereas the electronic position q and momentum p are d -dimensional vectors. The nuclear and electronic mass matrices, M and m , can, in general, be real symmetric $D \times D$ and $d \times d$ matrices, respectively.

The *time-dependent Hartree* (TDH)^{57,80–84} approximation is an optimal approximate solution to the molecular TDSE (1) among those in which the molecular state can be written as the Hartree product

$$\Psi_t = a_t \chi_t \psi_t \quad (5)$$

of the nuclear wavepacket χ_t and electronic wavepacket ψ_t ; the complex number a_t is inserted for convenience. In the TDH approximation, obtained by applying the Dirac-Frenkel time-dependent variational principle^{57,85,86} to ansatz (5), the prefactor evolves as⁵⁷

$$a_t = e^{iEt/\hbar}, \quad (6)$$

and the nuclear and electronic states satisfy the system

$$i\hbar \dot{\chi}_t = \hat{H}_{\text{nu}} \chi_t, \quad (7)$$

$$i\hbar \dot{\psi}_t = \hat{H}_{\text{el}} \psi_t. \quad (8)$$

of coupled nonlinear Schrödinger equations with mean-field nuclear and electronic Hamiltonian operators

$$\hat{H}_{\text{nu}} := \langle \mathcal{H} \rangle_{\psi_t} = \langle \psi_t | \mathcal{H} | \psi_t \rangle, \quad (9)$$

$$\hat{H}_{\text{el}} := \langle \mathcal{H} \rangle_{\chi_t} = \langle \chi_t | \mathcal{H} | \chi_t \rangle. \quad (10)$$

The mean-field operators satisfy the obvious identity $\langle \hat{H}_{\text{nu}} \rangle_{\chi_t} = \langle \hat{H}_{\text{el}} \rangle_{\psi_t} = E$. Note that the solution expressed by Eqs. (6)-(8) is unique except for an obvious gauge freedom in redistributing the phase among a_t , χ_t , and ψ_t .

B. Mixed quantum-classical limit: Ehrenfest dynamics

In the classical limit for nuclei, the nuclear position and momentum operators \hat{Q} and \hat{P} are replaced with classical variables Q and P . Then, the mean-field nuclear Hamiltonian (9) is no longer an operator, but a phase space function

$$H_{\text{nu}}(Q, P) = \langle \mathcal{H}(Q, P) \rangle_{\psi_t}, \quad (11)$$

where $\mathcal{H}(Q, P) = \hat{T}_{\text{el}} + T_{\text{nu}}(P) + \hat{V}(Q)$, and the mean-field electronic Hamiltonian (10) becomes the molecular Hamiltonian evaluated at the current nuclear positions and momenta:

$$\hat{H}_{\text{el}}(Q_t, P_t) = \mathcal{H}(Q_t, P_t). \quad (12)$$

We thus obtain the mixed quantum-classical Ehrenfest dynamics, in which the nuclear positions and momenta evolve according to classical Hamilton's equations of motion with Hamiltonian $H_{\text{nu}}(Q, P)$, and the electronic state evolves according to the TDSE with a time-dependent Hamiltonian $\hat{H}_{\text{el}}(Q_t, P_t)$:

$$\dot{Q}_t = \frac{\partial H_{\text{nu}}}{\partial P}(Q_t, P_t), \quad (13)$$

$$\dot{P}_t = -\frac{\partial H_{\text{nu}}}{\partial Q}(Q_t, P_t), \quad (14)$$

$$i\hbar\dot{\psi}_t = \hat{H}_{\text{el}}(Q_t, P_t)\psi_t. \quad (15)$$

Note that these three differential equations are coupled and, moreover, that the electronic TDSE is nonlinear due to this coupling.

Equations (13)–(15) can be re-expressed as more compact Hamilton's equations

$$\dot{q}_{\text{eff},t} = \frac{\partial H_{\text{eff}}}{\partial p_{\text{eff}}}(q_{\text{eff},t}, p_{\text{eff},t}), \quad (16)$$

$$\dot{p}_{\text{eff},t} = -\frac{\partial H_{\text{eff}}}{\partial q_{\text{eff}}}(q_{\text{eff},t}, p_{\text{eff},t}) \quad (17)$$

associated with an effective mixed quantum-classical Hamiltonian

$$\begin{aligned} H_{\text{eff}}(x_{\text{eff}}) &:= \langle \hat{H}_{\text{el}}(Q, P) \rangle_{\psi} \\ &= \frac{1}{2\hbar} [\langle \hat{H}_{\text{el}}(Q, P) \rangle_{q_{\psi}} + \langle \hat{H}_{\text{el}}(Q, P) \rangle_{p_{\psi}}], \end{aligned} \quad (18)$$

acting on an extended, effective mixed quantum-classical phase space with coordinates $x_{\text{eff}} = (q_{\text{eff}}, p_{\text{eff}}) = (Q, q_{\psi}, P, p_{\psi})$. The “quantum” Darboux coordinates (q_{ψ}, p_{ψ}) consist of the

real and imaginary part of the electronic wavefunction in position representation: $q_\psi := \sqrt{2\hbar}\text{Re}\psi(q)$ and $p_\psi := \sqrt{2\hbar}\text{Im}\psi(q)$ (we omit the dependence of q_ψ and p_ψ on q for brevity).

In general, q_ψ and p_ψ are real functions in an infinite-dimensional space; therefore, the “quantum” part

$$\dot{q}_{\psi,t} = \frac{\delta H_{\text{eff}}}{\delta p_\psi}(q_{\text{eff},t}, p_{\text{eff},t}), \quad (19)$$

$$\dot{p}_{\psi,t} = -\frac{\delta H_{\text{eff}}}{\delta q_\psi}(q_{\text{eff},t}, p_{\text{eff},t}) \quad (20)$$

of Eqs. (16) and (17), in fact, involves partial functional derivatives:⁸⁷

$$\begin{aligned} \frac{\delta H_{\text{eff}}}{\delta q_\psi} &= \frac{1}{2\hbar} \frac{\delta}{\delta q_\psi} \int [q_\psi \hat{H}_{\text{el}}(Q, P) q_\psi + p_\psi \hat{H}_{\text{el}}(Q, P) p_\psi] dq \\ &= \hbar^{-1} \hat{H}_{\text{el}}(Q, P) q_\psi, \end{aligned} \quad (21)$$

$$\begin{aligned} \frac{\delta H_{\text{eff}}}{\delta p_\psi} &= \frac{1}{2\hbar} \frac{\delta}{\delta p_\psi} \int [q_\psi \hat{H}_{\text{el}}(Q, P) q_\psi + p_\psi \hat{H}_{\text{el}}(Q, P) p_\psi] dq \\ &= \hbar^{-1} \hat{H}_{\text{el}}(Q, P) p_\psi. \end{aligned} \quad (22)$$

Substituting Eqs. (21) and (22) into Hamilton’s equations (19) and (20) recovers the TDSE (15) for the electronic wavefunction.

In practical calculations, q_ψ and p_ψ are usually represented in a finite basis or on a grid as N -dimensional vectors, where N is either the size of the basis or number of grid points. In such cases, functional derivatives (21) and (22) reduce to partial derivatives

$$\begin{aligned} \frac{\partial H_{\text{eff}}}{\partial q_\psi} &= \frac{1}{2\hbar} \frac{\partial}{\partial q_\psi} [q_\psi^T H_{\text{el}}(Q, P) q_\psi + p_\psi^T H_{\text{el}}(Q, P) p_\psi] \\ &= \hbar^{-1} H_{\text{el}}(Q, P) q_\psi, \end{aligned} \quad (23)$$

$$\begin{aligned} \frac{\partial H_{\text{eff}}}{\partial p_\psi} &= \frac{1}{2\hbar} \frac{\partial}{\partial p_\psi} [q_\psi^T H_{\text{el}}(Q, P) q_\psi + p_\psi^T H_{\text{el}}(Q, P) p_\psi] \\ &= \hbar^{-1} H_{\text{el}}(Q, P) p_\psi, \end{aligned} \quad (24)$$

where $H_{\text{el}}(Q, P)$ is an $N \times N$ matrix representation of operator $\hat{H}_{\text{el}}(Q, P)$.

C. Geometric properties

1. Norm conservation

Ehrenfest dynamics conserves the norm

$$\|\psi_t\| := \langle \psi_t | \psi_t \rangle^{1/2} \quad (25)$$

of the electronic wavefunction because

$$\begin{aligned}\frac{d}{dt}\|\psi_t\|^2 &= \langle \dot{\psi}_t | \psi_t \rangle + \langle \psi_t | \dot{\psi}_t \rangle \\ &= \frac{i}{\hbar} [\langle \hat{H}_{\text{el}}(Q_t, P_t) \rangle_{\psi_t} - \langle \hat{H}_{\text{el}}(Q_t, P_t) \rangle_{\psi_t}] = 0,\end{aligned}\quad (26)$$

where we used Eq. (15) and the hermiticity of $\hat{H}_{\text{el}}(Q_t, P_t)$.

2. Energy conservation

The total energy $E = H_{\text{nu}}(Q_t, P_t) = \langle \hat{H}_{\text{el}}(Q_t, P_t) \rangle_{\psi_t}$ of the system is conserved, in general, by the time-dependent variational principle and, in particular, by the TDH approximation. However, because we have also taken the mixed quantum-classical limit, let us verify the conservation of energy explicitly:

$$\begin{aligned}\frac{dE}{dt} &= \langle \dot{\psi}_t | \hat{H}_{\text{el}}(Q_t, P_t) | \psi_t \rangle + \langle \psi_t | \hat{H}_{\text{el}}(Q_t, P_t) | \dot{\psi}_t \rangle \\ &\quad + \dot{Q}_t^T \cdot \frac{\partial H_{\text{nu}}}{\partial Q}(Q_t, P_t) + \dot{P}_t^T \cdot \frac{\partial H_{\text{nu}}}{\partial P}(Q_t, P_t) \\ &= i\hbar[\langle \dot{\psi}_t | \dot{\psi}_t \rangle - \langle \dot{\psi}_t | \dot{\psi}_t \rangle] - \dot{Q}_t^T \cdot \dot{P}_t + \dot{P}_t^T \cdot \dot{Q}_t = 0,\end{aligned}\quad (27)$$

where we used the hermiticity of $\hat{H}_{\text{el}}(Q_t, P_t)$ and Eqs. (13)–(15). The energy conservation also follows directly from the effective Hamiltonian structure:

$$\begin{aligned}\frac{dE}{dt} &= \frac{d}{dt} H_{\text{eff}}(q_{\text{eff},t}, p_{\text{eff},t}) \\ &= \dot{q}_{\text{eff},t}^T \frac{\partial H_{\text{eff}}}{\partial q_{\text{eff}}}(q_{\text{eff},t}, p_{\text{eff},t}) + \dot{p}_{\text{eff},t}^T \frac{\partial H_{\text{eff}}}{\partial p_{\text{eff}}}(q_{\text{eff},t}, p_{\text{eff},t}) \\ &= -\dot{q}_{\text{eff},t}^T \dot{p}_{\text{eff},t} + \dot{p}_{\text{eff},t}^T \dot{q}_{\text{eff},t} = 0,\end{aligned}\quad (28)$$

where we used Eqs. (16) and (17).

3. Symplecticity

The effective, mixed quantum-classical symplectic two-form

$$\omega_{\text{eff}} := dq_{\text{eff}} \wedge dp_{\text{eff}} = \omega_{\text{cl}} + \omega_{\text{qm}} \quad (29)$$

is a sum of the classical (cl) canonical two-form $\omega_{\text{cl}} := dQ \wedge dP$ and the quantum (qm) canonical two-form $\omega_{\text{qm}} := dq_{\psi} \wedge dp_{\psi}$, which acts on states ψ_1 and ψ_2 as $\omega_{\text{qm}}(\psi_1, \psi_2) =$

$2\hbar\text{Im}\langle\psi_1|\psi_2\rangle$ (see Appendix B and Refs. 57, 87, and 88). Let $\Phi_{H_{\text{eff}},t} : x_{\text{eff},0} \mapsto x_{\text{eff},t}$ denote the Hamiltonian flow of H_{eff} . The stability (or Jacobian) matrix M_t of the Hamiltonian flow $\Phi_{H,t}$ is a symplectic matrix. While this holds in general,^{56,89} we show it explicitly for our case in Appendix C. As a result, Ehrenfest dynamics conserves the symplectic two-form ω_{eff} from Eq. (29) (see Appendix C).

4. Time reversibility

An involution is a mapping S that is its own inverse, i.e., $S(S(x)) = x$. We will consider the involution

$$S = \begin{pmatrix} I_{D+N} & 0 \\ 0 & -I_{D+N} \end{pmatrix} \quad (30)$$

that changes the sign of the nuclear momenta and conjugates the electronic wavefunction in position representation (i.e., changes the sign of p_ψ). Following Ref. 56, we call a flow Φ_t time-reversible under a general involution S if it satisfies

$$S\Phi_t[S\Phi_t(x_{\text{eff}})] = x_{\text{eff}}. \quad (31)$$

Because effective Hamiltonian H_{eff} is an even function in p_{eff} , i.e., $H_{\text{eff}}(x_{\text{eff}}) = H_{\text{eff}}(Sx_{\text{eff}})$, its Hamiltonian flow satisfies⁵⁶

$$\Phi_{H_{\text{eff}},t}(x_{\text{eff}}) = S\Phi_{H_{\text{eff}},-t}(Sx_{\text{eff}}). \quad (32)$$

Since $S^{-1} = S$ and, by definition, any flow is symmetric (i.e., $\Phi_{-t} = \Phi_t^{-1}$),^{55,56} the satisfaction of Eq. (32) implies the satisfaction of the time reversibility condition (31).

D. Geometric Integrators

As in the split-operator algorithm^{61,90–92} for the TDSE or in the Verlet algorithm⁶² for Hamilton's equations of motion, we can obtain a symmetric potential-kinetic-potential (VTV) algorithm of the second order in the time step Δt by using the Strang splitting⁵⁹ and performing, in sequence, potential propagation for time $\Delta t/2$, kinetic propagation for Δt , and potential propagation for $\Delta t/2$. The second-order kinetic-potential-kinetic (TVT) algorithm is obtained similarly, by exchanging the potential and kinetic propagations. Either of the two second-order algorithms can be symmetrically composed^{55,93} to obtain an algorithm

of an arbitrary even order of accuracy in Δt . This is achieved by using the recursive triple-jump^{70,71} or Suzuki-fractal⁷¹ composition schemes, or with a more efficient scheme specific to each order (which we shall call “optimal”).^{71,73,74} We, therefore, only need to present the analytical solutions of the kinetic and potential propagation steps for arbitrary times t .

During the kinetic propagation, the Hamiltonian reduces to

$$\hat{H}(Q, P) = \hat{T}_{\text{el}} + T_{\text{nu}}(P), \quad (33)$$

and the equations of motion (13)–(15) become

$$\dot{Q}_t = M^{-1} \cdot P_t, \quad (34)$$

$$\dot{P}_t = 0, \quad (35)$$

$$i\hbar\dot{\psi}_t = [\hat{T}_{\text{el}} + T_{\text{nu}}(P_t)]\psi_t, \quad (36)$$

which are equivalent to Hamilton’s equations (16) and (17) with $H_{\text{eff}} = \langle \hat{T}_{\text{el}} + T_{\text{nu}}(P) \rangle_{\psi}$. Because nuclear momenta P_t do not evolve during the kinetic propagation, Eqs. (34)–(36) can be solved analytically to obtain

$$Q_t = Q_0 + tM^{-1} \cdot P_0, \quad (37)$$

$$P_t = P_0, \quad (38)$$

$$\psi_t = e^{-it[\hat{T}_{\text{el}} + T_{\text{nu}}(P_0)]/\hbar}\psi_0. \quad (39)$$

As $\hat{T}_{\text{el}} = T(\hat{p})$, Eq. (39) is easily evaluated in momentum representation.

During the potential propagation, the Hamiltonian reduces to

$$\hat{H}(Q, P) = \hat{V}(Q), \quad (40)$$

and the equations of motion (13)–(15) become

$$\dot{Q}_t = 0, \quad (41)$$

$$\dot{P}_t = -\langle \hat{V}'(Q_t) \rangle_{\psi_t}, \quad (42)$$

$$i\hbar\dot{\psi}_t = \hat{V}(Q_t)\psi_t, \quad (43)$$

which are equivalent to Hamilton’s equations (16) and (17) with $H_{\text{eff}} = \langle \hat{V}(Q) \rangle_{\psi}$. Because nuclear positions Q_t do not evolve during the potential propagation, one can replace Q_t with Q_0 in Eqs. (42) and (43). Even after the substitution of $Q_t = Q_0$, Eq. (42) seems hard to

solve due to an apparent coupling to Eq. (43). However, this coupling can be removed by noting that

$$\begin{aligned}
\langle \hat{V}'(Q_0) \rangle_{\psi_t} &= \langle \psi_0 | e^{it\hat{V}(Q_0)/\hbar} \hat{V}'(Q_0) e^{-it\hat{V}(Q_0)/\hbar} | \psi_0 \rangle \\
&= \langle \psi_0 | e^{it\hat{V}(Q_0)/\hbar} e^{-it\hat{V}(Q_0)/\hbar} \hat{V}'(Q_0) | \psi_0 \rangle \\
&= \langle \hat{V}'(Q_0) \rangle_{\psi_0}.
\end{aligned} \tag{44}$$

As a result, Eqs. (41)–(43) can be solved analytically to obtain

$$Q_t = Q_0, \tag{45}$$

$$P_t = P_0 - t \langle \hat{V}'(Q_0) \rangle_{\psi_0}, \tag{46}$$

$$\psi_t = e^{-it\hat{V}(Q_0)/\hbar} \psi_0. \tag{47}$$

As $\hat{V}(Q) = V(\hat{q}, Q)$, Eq. (47) is easily evaluated in position representation.

E. Geometric properties of the geometric integrator

Like all other integrators obtained with the splitting method, in the proposed algorithm, each potential or kinetic step of the Ehrenfest dynamics is solved exactly, and each of these steps has all the geometric properties of the exact solution. The second-order Strang splitting method, composed from two exact flows, or any of its symmetric compositions preserves all the listed geometric properties except the conservation of energy (see, e.g., Refs. 55 and 56 or Refs. 91–93 and references therein).

III. NUMERICAL EXAMPLE

We use a low-dimensional model that is solvable “numerically” exactly to demonstrate the geometric and convergence properties of the presented integrators. Since the high efficiency and geometric properties of these integrators are most meaningful when the mean-field Ehrenfest approximation is valid, we have chosen the system and initial state carefully so that numerically converged Ehrenfest and exact quantum simulations yield similar results. At the same time, we have ensured that the resulting nonadiabatic simulation describes a realistic light-induced excitation. (See references in Sec. I for higher-dimensional examples where the Ehrenfest approximation was employed successfully.)

The four-dimensional extension^{75–77} of the Shin–Metiu model^{78,79} consists of an interacting electron and proton, both moving in two spatial dimensions and feeling an additional field of two fixed protons (all three protons are distinguishable). The four-dimensional ($D = 2$, $d = 2$) model Hamiltonian is of form (2) with

$$\begin{aligned} \mathcal{V} = & V_{\text{quartic}}(\hat{Q}) + V^{en}(|\hat{q} - Q_a|) + V^{en}(|\hat{q} - Q_b|) \\ & + V^{en}(|\hat{q} - \hat{Q}|) + V^{nn}(|\hat{Q} - Q_a|) \\ & + V^{nn}(|\hat{Q} - Q_b|) + V^{nn}(|Q_a - Q_b|), \end{aligned} \quad (48)$$

where $Q_a = (-L/2, 0)$ and $Q_b = (L/2, 0)$ are the positions of the two fixed protons, and

$$V^{en}(\xi) = -1/\sqrt{a + \xi^2} \quad (49)$$

$$V^{nn}(\xi) = 1/\sqrt{b + \xi^2} \quad (50)$$

are attractive and repulsive regularized Coulomb potentials; following Ref. 75, we take $L = 4\sqrt{3}/5$ a.u., $a = 0.5$ (a.u.)², and $b = 10$ (a.u.)². Quartic potential $V_{\text{quartic}}(Q) = (|Q|/Q_c)^4$ with $Q_c = 3.5$ a.u. ensures that the system remains bound.

For the dynamics, we considered the initial state

$$\Psi_0(q, Q) = \chi_{\text{gwp}}(Q - Q_0)\varphi_2(q; Q), \quad (51)$$

where φ_i is the i th excited adiabatic electronic state, and

$$\chi_{\text{gwp}}(Q) = \frac{1}{\sqrt{\pi\hbar\sigma^2}} e^{-Q^2/(2\hbar\sigma^2)} \quad (52)$$

is the ground vibrational eigenstate of a harmonic fit to the ground electronic state; here, $\sigma = 0.24$ a.u. The displacement of the initial wavepacket by $Q_0 = (0.5 \text{ a.u.}, 1.5 \text{ a.u.})$ from the ground state equilibrium is motivated by the displaced excitation of molecules: Suppose state φ_2 is dark; then a wavepacket may reach it at a nuclear geometry that is not the ground state equilibrium via an intersection with a bright state. To obtain $\varphi_2(q; Q)$, we solved the electronic time-independent Schrödinger equation

$$[\hat{T}_{\text{el}} + \hat{V}(Q)]\varphi_i(Q) = E_i(Q)\varphi_i(Q), \quad (53)$$

where $\hat{T}_{\text{el}} = T(\hat{p})$ and $\hat{V}(Q) = V(\hat{q}, Q)$ are operators acting on electrons; in position representation, Eq. (53) takes a more familiar form

$$\left[-\frac{\hbar^2}{2m} \frac{\partial^2}{\partial q^2} + V(q; Q) \right] \varphi_i(q; Q) = E_i(Q)\varphi_i(q; Q). \quad (54)$$

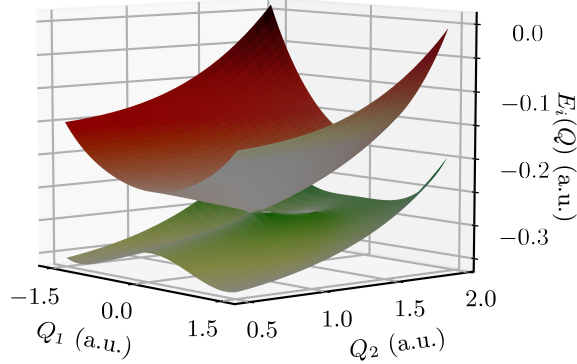


FIG. 1. Potential energy surfaces in the vicinity of the conical intersection at $Q = Q_{\text{CI}} = (0, 1.2 \text{ a.u.})$ in the model system from Sec. III. Energies $E_i(Q) := \langle \varphi_i(Q) | \hat{T}_{\text{el}} + \hat{V}(Q) | \varphi_i(Q) \rangle$ of the first ($i = 1$) and second ($i = 2$) excited adiabatic electronic states $\varphi_i(Q)$ are shown in green and red, respectively.

Section S1 of the supplementary material describes the method we employed to solve this equation.

Because our approach does not rely on a specific electronic basis (such as the basis of adiabatic or diabatic electronic states) to represent the molecular wavepacket, the initial state can be a general function of q and Q . To be specific, however, we chose to start the dynamics from a single excited adiabatic electronic state (here φ_2), which is the most common choice in the literature studying nonadiabatic dynamics following a light-induced excitation.^{27,94–97} In the model described by Eqs. (48)–(50), the second excited adiabatic state φ_2 is, indeed, significantly coupled to the first excited state φ_1 by a conical intersection depicted in Fig. 1.

In Fig. 2, we compare the exact quantum dynamics $\Psi_t = \exp(-it\mathcal{H}/\hbar)\Psi_0$ with Ehrenfest dynamics $x_{\text{eff},t} = \Phi_{H_{\text{eff},t}}(x_{\text{eff},0})$. The initial state of the system is $(Q_t, P_t, \psi_t)|_{t=0} = (Q_0, 0, \varphi_2(Q_0))$ and the corresponding initial mixed quantum-classical phase space point

$$x_{\text{eff},0} = (Q_0, \sqrt{2\hbar}\text{Re}\varphi_2(q; Q_0), 0, 0) \quad (55)$$

can be thought of as state (51) with an infinitesimally narrow Gaussian wavepacket; the fourth component in Eq. (55) is zero because the state $\varphi_2(q; Q_0)$, in position representation, is purely real: $\text{Im}\varphi_2(q; Q_0) = 0$. We compare three observables: nuclear position $Q(t)$, adiabatic population $\mathcal{P}_i(t)$, and electronic density $\rho_{\text{el}}(q, t)$. In quantum dynamics, they are

obtained from the full wavefunction Ψ_t as^{75,77}

$$Q(t) = \langle \hat{Q} \rangle_{\Psi_t}, \quad (56)$$

$$\mathcal{P}_i(t) = \langle \hat{\mathcal{P}}_i \rangle_{\Psi_t}, \quad (57)$$

$$\rho_{\text{el}}(q, t) = \int dQ |\Psi_t(q, Q)|^2. \quad (58)$$

To find population $\mathcal{P}_i(t)$ from Eq. (57), we computed the expectation value of the population operator $\hat{\mathcal{P}}_i := |\varphi_i\rangle\langle\varphi_i|$ in position representation:⁷⁷

$$\langle \hat{\mathcal{P}}_i \rangle_{\Psi_t} = \int \left| \int \varphi_i(q; Q)^* \Psi_t(q, Q) dq \right|^2 dQ. \quad (59)$$

In Ehrenfest dynamics, the nuclear position $Q(t)$ is simply the current position Q_t of the trajectory, whereas the adiabatic population $\mathcal{P}_i(t) = |\langle \varphi_i(Q_t) | \psi_t \rangle|^2$ and electronic density $\rho_{\text{el}}(q, t) = |\psi_t(q)|^2$ depend on the electronic wavefunction ψ_t .

Figure 2 shows that during the considered time interval $t \in [0, t_f]$ with $t_f = 170$ a.u., Ehrenfest dynamics yields qualitatively correct results. In particular, the nuclear motion towards the conical intersection at $Q = Q_{\text{CI}} = (0, 1.2 \text{ a.u.})$ [panels (a) and (b)] and the resulting population transfer from the initial second excited to the first excited state [panels (c) and (d)] are well described by Ehrenfest dynamics. The electronic densities obtained from the exact quantum and Ehrenfest dynamics [panels (e) and (f)] at the final time $t = t_f$ are also very similar. The mean-field Ehrenfest approximation works well because the nuclear density remains localized (not shown) and the electronic density is almost stationary.

In the following, we demonstrate the geometric properties and high efficiency of high-order geometric integrators (from Sec. II D). Owing to the low electronic dimensionality ($d = 2$) of the employed model, we could ensure that the numerical errors due to the representation of the electronic wavefunction $\psi_t(q)$ were negligible in comparison with the time propagation errors: The wavefunction was represented, with high accuracy, on a uniform grid (see Sec. S1 of the supplementary material for computational details). This approach, however, would be too computationally demanding in practical, higher-dimensional (i.e., larger d) simulations. Instead, for such simulations, one of the real-time time-dependent electronic structure methods,^{68,69} such as real-time time-dependent Hartree–Fock (TDHF)^{11,13,98} and real-time time-dependent density functional theory (TDDFT),^{99–106} should be employed. In particular, because there are existing implementations of real-time TDDFT using the split-operator algorithms for the propagation of Kohn–Sham orbitals,^{107–111} it should be straightforward to

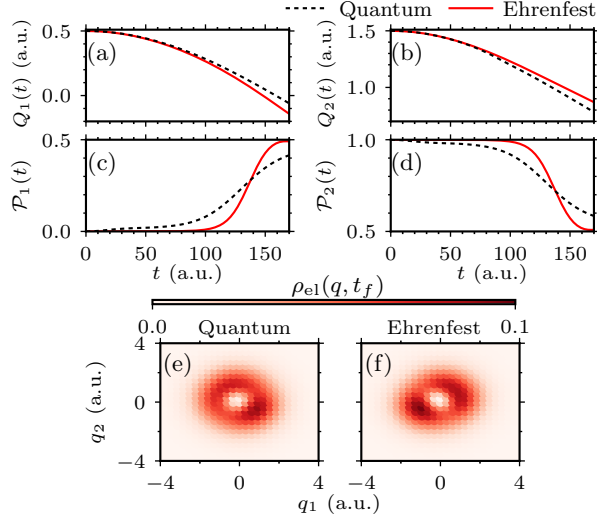


FIG. 2. Comparison of Ehrenfest dynamics with the exact quantum dynamics. (a)–(d): Time dependence of nuclear position $Q_n(t)$ [$n = 1$ in panel (a), $n = 2$ in panel (b)] and of the first and second excited adiabatic populations $\mathcal{P}_i(t)$ [$i = 1$ in panel (c), $i = 2$ in panel (d)]. (e) and (f): Electronic densities at the final time $t = t_f$ obtained from quantum dynamics [panel (e)] and Ehrenfest dynamics [panel (f)].

employ the presented integrators for TDDFT-Ehrenfest simulations. However, the exact efficiency of the high-order geometric integrators when applied to realistic TDDFT-Ehrenfest simulations is hard to predict and is outside the scope of this study.

In Fig. 3, we demonstrate the geometric properties of the presented integrators (in all figures, we omit the results of the TVT algorithm and its compositions because they are nearly identical to the corresponding results for the VTV algorithm). The figure shows that the norm of the electronic wavefunction [panels (a) and (b)], time reversibility [panels (c) and (d)], and symplecticity [panels (e) and (f)] are conserved as functions of time [for a fixed time step $\Delta t = 0.5$ a.u., panels (a), (c), and (e)] and regardless of the time step Δt used [for a fixed final time $t_f = 170$ a.u., panels (b), (d), and (f)]. We check the symplecticity of stability matrix M_t by measuring the Frobenius distance

$$d_t = \|M_t^T J M_t - J\| \quad (60)$$

of $M_t^T J M_t$ from J (see Appendix C). Here,

$$J := \begin{pmatrix} 0 & -I_{D+N} \\ I_{D+N} & 0 \end{pmatrix} \quad (61)$$

is the *standard symplectic matrix*, and the Frobenius norm is defined as $\|A\| := \langle A, A \rangle^{1/2}$, where $\langle A, B \rangle := \text{Tr}(A^\dagger B)$. Time reversibility of an approximate method that approximates the exact flow Φ_t at discrete times $t = n\Delta t$ (n integer) by an iterated map $\Phi_{\text{appr},t}^{(\Delta t)} := (\Phi_{\text{appr}}^{(\Delta t)})^n : x_{\text{eff},0} \mapsto x_{\text{eff},t}^{(\Delta t)}$ is measured by the distance

$$\mathcal{T}_t := \|x_{\text{eff},t}^{\text{fb}} - x_{\text{eff},0}\| \quad (62)$$

of the forward-backward propagated state $x_{\text{eff},t}^{\text{fb}} := S\Phi_{\text{appr},t}^{(\Delta t)}[S\Phi_{\text{appr},t}^{(\Delta t)}(x_{\text{eff},0})]$ from the initial state $x_{\text{eff},0}$. The norm $\|x_{\text{eff}}\| := \langle x_{\text{eff}}, x_{\text{eff}} \rangle^{1/2}$ of an effective phase space point x_{eff} is defined using the scalar product $\langle x_{\text{eff},1}, x_{\text{eff},2} \rangle := Q_1^T \cdot Q_2 + P_1^T \cdot P_2 + \langle \psi_1 | \psi_2 \rangle$ of $x_{\text{eff},1}$ and $x_{\text{eff},2}$. The corresponding squared “distance” $\|x_{\text{eff},1} - x_{\text{eff},2}\|^2$ between points $x_{\text{eff},1}$ and $x_{\text{eff},2}$ is simply the sum $\|Q_1 - Q_2\|^2 + \|P_1 - P_2\|^2 + \|\psi_1 - \psi_2\|^2$ of the squared distances between Q_1 and Q_2 , between P_1 and P_2 , and between ψ_1 and ψ_2 .

Panels (g) and (h) of Fig. 3 show that the energy is only conserved approximately, to the same order as the order of convergence of the integrator. The loss of exact energy conservation is standard for any splitting method^{55,91} and is due to alternating kinetic and potential propagations: the effective Hamiltonian alternates between $H_{\text{eff}} = \langle \hat{T}_{\text{el}} + T_{\text{nu}}(P) \rangle_\psi$ and $H_{\text{eff}} = \langle \hat{V}(Q) \rangle_\psi$, and its time-dependent nature breaks the conservation of energy.

Figure 4 confirms the predicted asymptotic order of convergence of the geometric integrators. However, panel (c) may wrongly suggest that the Suzuki-fractal scheme leads to the most efficient method, as it has the smallest error for each time step size. What Fig. 4 does not show is that the sixth-order Suzuki-fractal scheme has a factor of 25/9 more sub-steps per time step than either the triple-jump or optimal scheme. If we instead consider the dependence of the convergence error on the computational cost [measured by the central processing unit (CPU) time], the optimal composition scheme indeed yields the most efficient method for each order of accuracy (see Fig. S1 in Sec. S2 of the supplementary material).

To reach a modest convergence error of 10^{-3} , the most efficient geometric integrator (obtained using the optimal fourth-order composition scheme) is 15 times faster than the two time step method and roughly twice slower than the three time step method (see Fig. 5). Yet, a clear advantage of the geometric integrators over the other methods is the exact conservation of geometric properties. Both the two and three time step methods violate symplecticity; the two time step method, in addition, violates time reversibility (see Fig. 6

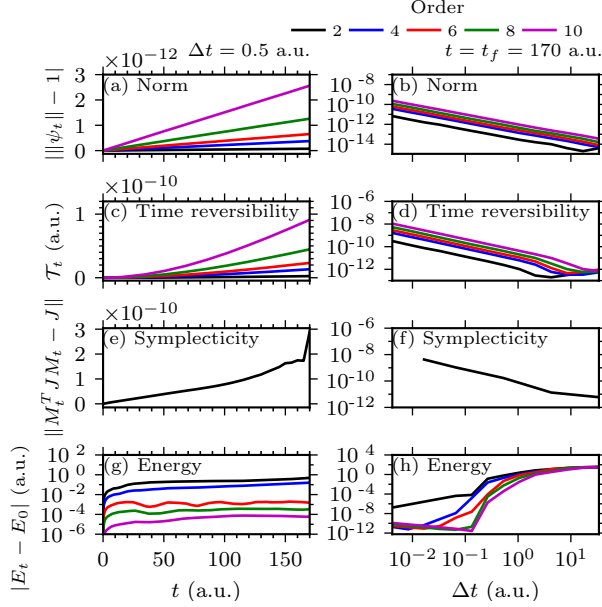


FIG. 3. Conservation of geometric properties by the geometric integrators presented in Sec. II D. (a) and (b): Norm of the electronic wavefunction. (c) and (d): Time reversibility [Eq. (62)]. (e) and (f): Symplecticity [Eq. (60)]. (g) and (h): Energy. Both the time dependence of the geometric properties for a fixed time step $\Delta t = 0.5$ a.u. [left-hand side panels (a), (c), (e), and (g)] and the geometric properties at the final time, $t = t_f = 170$ a.u., as functions of Δt [right-hand side panels (b), (d), (f), and (h)] are shown. The costly numerical propagation of stability matrix M_t is done separately from the main Ehrenfest dynamics (see Appendix D). Due to prohibitive computational cost, only the elementary second-order method is presented in panels (e) and (f); however, all of its compositions are symplectic regardless of the time step (as justified in Sec. II E). Initial energy of the system is $E_0 = -0.2$ a.u. To avoid clutter, only the higher-order integrators obtained using the optimal composition schemes are shown (the Suzuki-fractal scheme is the optimal fourth-order scheme⁹³).

in Appendix A). Moreover, due to its higher order of convergence in Δt , the fourth-order geometric integrator becomes more efficient than even the three time step method to reach convergence errors below 10^{-4} (see Fig. 5).

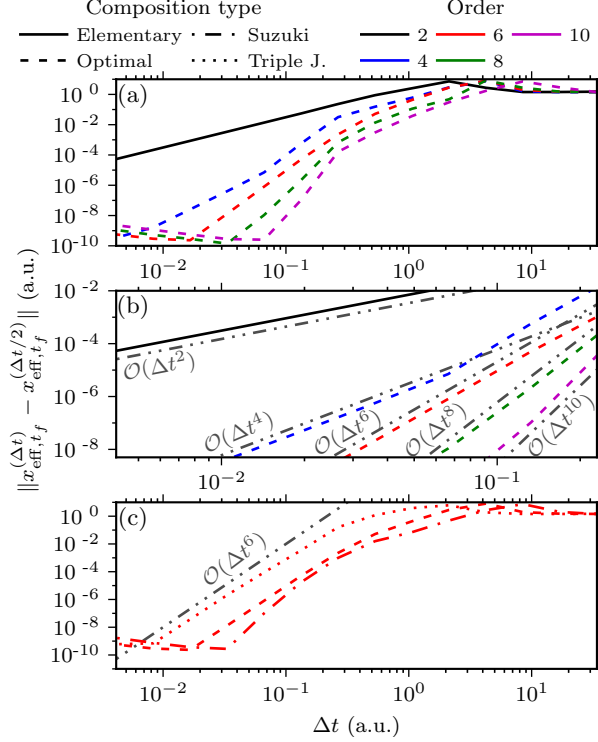


FIG. 4. Convergence of geometric integrators for Ehrenfest dynamics measured by the convergence error of the final effective phase space point x_{eff,t_f} as a function of Δt . Gray straight lines indicate various predicted orders of convergence $\mathcal{O}(\Delta t^n)$. (a) Methods obtained using the optimal composition schemes, i.e., methods presented in Fig. 3. (b) Zoomed-in version of panel (a), highlighting the asymptotic orders of convergence of the integrators. (c) Sixth-order methods obtained using the triple jump, Suzuki-fractal, and optimal composition schemes. The error of an approximate method is measured by the distance $\|x_{\text{eff},t_f}^{(\Delta t)} - x_{\text{eff},t_f}^{(\Delta t/2)}\|$ of the final point $x_{\text{eff},t_f}^{(\Delta t)} = \Phi_{\text{appr},t_f}^{(\Delta t)}(x_{\text{eff},0})$, obtained with time step Δt , from the final point $x_{\text{eff},t_f}^{(\Delta t/2)} = \Phi_{\text{appr},t_f}^{(\Delta t/2)}(x_{\text{eff},0})$, obtained with half time step $\Delta t/2$.

IV. CONCLUSION

We have demonstrated that the high-order geometric integrators for Ehrenfest dynamics can be obtained by simultaneously employing the splitting and composition methods. Since Ehrenfest dynamics already involves a rather severe approximation, one is often not interested in numerically converged solutions. In such cases, geometric integrators become much more relevant because only they guarantee the exact conservation of the geometric invariants regardless of the accuracy of the solution.

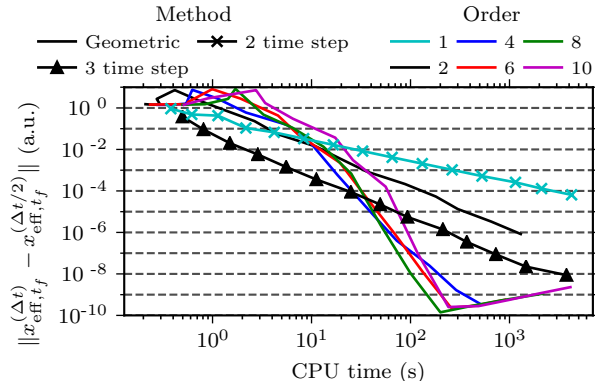


FIG. 5. Efficiency of the geometric integrators is compared with the efficiency of the widely-used two time step and three time step methods. Efficiency is measured using the dependence of the convergence error on the computational cost. Only the higher-order geometric integrators obtained using the optimal composition schemes are shown, for they are the most efficient for each order of accuracy.

That is not to say that the high-order geometric integrators are inefficient for high accuracy simulations. On the contrary, to reach an error of, e.g., 10^{-6} , using the eighth-order geometric integrator yields a four-fold speedup over the three time step method (see Fig. 5) and a 5000-fold speedup over the two time step method. High-accuracy results with negligible numerical errors may be desirable when the error introduced by the mean-field Ehrenfest approximation is either very small or unknown.

SUPPLEMENTARY MATERIAL

See the supplementary material for the computational details (Sec. S1), efficiency of the high-order geometric integrators obtained using the triple-jump, Suzuki-fractal, optimal composition schemes (Sec. S2), and detailed algorithms of the two and three time step methods (Sec. S3).

ACKNOWLEDGMENTS

The authors acknowledge the financial support from the European Research Council (ERC) under the European Union’s Horizon 2020 research and innovation programme (grant

agreement No. 683069 – MOLEQULE) and thank Tomislav Begušić and Nikolay Golubev for useful discussions.

AUTHOR DECLARATIONS

Conflict of interest

The authors have no conflicts to disclose.

DATA AVAILABILITY

The data that support the findings of this study are openly available in Zenodo at <https://doi.org/10.5281/zenodo.5167211>.

Appendix A: Two and three time step methods

1. Two time step method

Unlike the geometric integrators, which propagate Q_t, P_t , and ψ_t simultaneously, the two time step method^{11,12,53} consists in alternately propagating the classical nuclear phase space point and electronic wavefunction. The time step $\Delta t_{\text{el}} = \Delta t/n_{\text{el}}$ for the electronic propagation is typically much smaller than the time step Δt for the nuclear propagation (we used $n_{\text{el}} = 100$).

In the two time step method, we employed the second-order Verlet algorithm⁶² to propagate the nuclear phase space point and the second-order VTV split-operator algorithm⁶¹ to propagate the electronic wavefunction. However, because the nuclear phase space point and electronic wavefunction are propagated separately and alternately, the overall two time step method is only first-order accurate in the time step. Moreover, the method is neither time-reversible nor symplectic (see Fig. 6). See Sec. S3 of the supplementary material for the detailed algorithm of the two time step method.

2. Three time step method

The three time step method,^{13,54} owing to its symmetry, is both time-reversible and second-order accurate in the time step.⁵⁵ However, the method is still not symplectic (see Fig. 6).

In addition to the nuclear time step Δt and electronic time step Δt_{el} , used also in the two time step method, the three time step method improves the efficiency by introducing the intermediate *nuclear-electronic coupling* time step $\Delta t_{\text{nu-el}} = \Delta t/n_{\text{nu-el}} = \Delta t_{\text{el}}n_{\text{el}}/n_{\text{nu-el}}$ (we used $n_{\text{nu-el}} = 10$). See Sec. S3 of the supplementary material for the detailed algorithm of the three time step method.

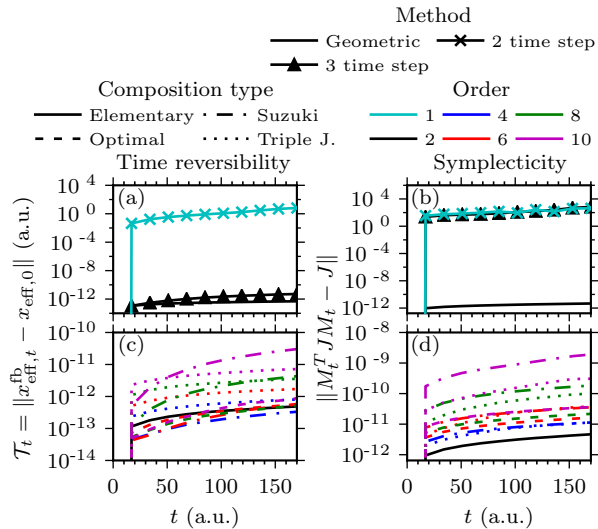


FIG. 6. Violation of (a) time reversibility [see Eq. (62)] and (b) symplecticity [see Eq. (60)] by the non-geometric integrators: The two time step method is neither reversible nor symplectic, whereas the three time step method is time-reversible but not symplectic. The geometric integrators exactly preserve both (c) time-reversibility and (d) symplecticity. Time step $\Delta t = 17$ a.u. was used. For the two and three time step methods, the corresponding convergence errors are 0.5 and 0.09, respectively, and for all of the presented geometric integrators, the errors are > 1.4 .

Appendix B: Quantum canonical two-form

The canonical two-form $dq_\psi \wedge dp_\psi$ acts on states ψ_1 and ψ_2 as

$$dq_\psi \wedge dp_\psi(\psi_1, \psi_2) = 2\hbar \text{Im}\langle \psi_1 | \psi_2 \rangle \quad (\text{B1})$$

because

$$\begin{aligned}
dq_\psi \wedge dp_\psi(\psi_1, \psi_2) &= \langle dq_\psi(\psi_1) | dp_\psi(\psi_2) \rangle - \langle dp_\psi(\psi_1) | dq_\psi(\psi_2) \rangle \\
&= 2\hbar[\langle \text{Re}\psi_1(q) | \text{Im}\psi_2(q) \rangle - \langle \text{Im}\psi_1(q) | \text{Re}\psi_2(q) \rangle] \\
&= 2\hbar \text{Im}\langle \psi_1 | \psi_2 \rangle,
\end{aligned} \tag{B2}$$

where we have used that the tangent space of a vector space can be identified with the vector space itself,¹¹² i.e.,

$$dq_\psi(\psi) = q_\psi = \sqrt{2\hbar} \text{Re}\psi(q), \tag{B3}$$

$$dp_\psi(\psi) = p_\psi = \sqrt{2\hbar} \text{Im}\psi(q). \tag{B4}$$

Appendix C: Symplecticity of the exact Hamiltonian flow

We use the *standard symplectic matrix*

$$J := \begin{pmatrix} 0 & -I_{D+N} \\ I_{D+N} & 0 \end{pmatrix} \tag{C1}$$

and re-express effective symplectic two-form (29) as⁵⁶

$$\omega_{\text{eff}} = \frac{1}{2} (J dx_{\text{eff}}) \wedge dx_{\text{eff}}. \tag{C2}$$

Since $dx_{\text{eff},t} = M_t dx_{\text{eff},0}$, we have

$$\begin{aligned}
(J dx_{\text{eff},t}) \wedge dx_{\text{eff},t} &= (J M_t dx_{\text{eff},0}) \wedge (M_t dx_{\text{eff},0}) \\
&= (M_t^T J M_t dx_{\text{eff},0}) \wedge dx_{\text{eff},0},
\end{aligned} \tag{C3}$$

and two-form ω_{eff} is conserved [i.e., $(J dx_{\text{eff},t}) \wedge dx_{\text{eff},t} = (J dx_{\text{eff},0}) \wedge dx_{\text{eff},0}$] if M_t is a symplectic matrix, i.e., if it satisfies the condition

$$M_t^T J M_t = J. \tag{C4}$$

Since $M_0 = I$, Eq. (C4) is trivially satisfied at $t = 0$. To show that the stability matrix M_t of Hamiltonian flow $\Phi_{H_{\text{eff},t}}$ is symplectic, we therefore only have to show that

$d(M_t^T J M_t)/dt = 0$, which follows easily from the calculation

$$\begin{aligned}
\frac{d}{dt} M_t^T J M_t &= \dot{M}_t^T J M_t + M_t^T J \dot{M}_t \\
&= M_t^T \text{Hess}[H_{\text{eff}}(x_{\text{eff},t})] J^2 M_t \\
&\quad + M_t^T J J^T \text{Hess}[H_{\text{eff}}(x_{\text{eff},t})] M_t \\
&= -M_t^T \text{Hess}[H_{\text{eff}}(x_{\text{eff},t})] M_t \\
&\quad + M_t^T \text{Hess}[H_{\text{eff}}(x_{\text{eff},t})] M_t \\
&= 0,
\end{aligned} \tag{C5}$$

where we have used the fact that the time derivative of the stability matrix satisfies⁵⁶

$$\dot{M}_t = J^T \text{Hess}[H_{\text{eff}}(x_{\text{eff},t})] M_t. \tag{C6}$$

Although we did not need the explicit form

$$\begin{aligned}
&\text{Hess}[H_{\text{eff}}(x_{\text{eff}})] = \\
&\left(\begin{array}{cccc}
\langle \text{Hess} \hat{V}(Q) \rangle_\psi & d_V(Q) q_\psi & 0 & d_V(Q) p_\psi \\
d_V(Q) q_\psi & \hat{H}_{\text{el}}(Q, P)/\hbar & d_T(P) q_\psi & 0 \\
0 & d_T(P) q_\psi & 1/M & d_T(P) p_\psi \\
d_V(Q) p_\psi & 0 & d_T(P) p_\psi & \hat{H}_{\text{el}}(Q, P)/\hbar
\end{array} \right)
\end{aligned} \tag{C7}$$

of the Hessian of $H_{\text{eff}}(x_{\text{eff}})$ to prove the symplecticity of M_t , this expression will be useful for the numerical propagation of the stability matrix; we defined and used

$$d_V(Q) := \hat{V}'(Q)/\hbar, \tag{C8}$$

$$d_T(P) := P/(\hbar M) \tag{C9}$$

to simplify Eq. (C7).

Appendix D: Numerical propagation of the stability matrix

The numerical propagation of stability matrix M_t requires much more computational effort than the propagation of mixed quantum-classical phase space point x_{eff} . It is, in general, not necessary to propagate the stability matrix to simulate Ehrenfest dynamics. Yet, to numerically demonstrate the symplecticity of the geometric integrators, i.e., to prepare

panels (e) and (f) of Fig. 3, we propagated also the stability matrix. Like in the propagation of x_{eff} , we only need to present the analytical solutions of the kinetic and potential propagation steps for arbitrary times t because all presented geometric integrators are composed of kinetic and potential propagations (see Sec. IID).

During the kinetic propagation, the equation of motion

$$\dot{M}_t = J^T \text{Hess}[\langle \hat{T}_{\text{nu+el}}(P_t) \rangle_{\psi_t}] M_t \quad (\text{D1})$$

for stability matrix M_t is obtained by reducing the effective Hamiltonian to $H_{\text{eff}}(x_{\text{eff}}) = \langle \hat{T}_{\text{nu+el}}(P) \rangle_{\psi} = \langle T_{\text{nu}}(P) + \hat{T}_{\text{el}} \rangle_{\psi}$ in Eq. (C6). The explicit form of the Hessian is

$$\text{Hess}[\langle \hat{T}_{\text{nu+el}}(P) \rangle_{\psi}] = \begin{pmatrix} 0 & 0 & 0 & 0 \\ 0 & \hat{T}_{\text{nu+el}}(P)/\hbar & d_T(P)q_{\psi} & 0 \\ 0 & d_T(P)q_{\psi} & 1/M & d_T(P)p_{\psi} \\ 0 & 0 & d_T(P)p_{\psi} & \hat{T}_{\text{nu+el}}(P)/\hbar \end{pmatrix}, \quad (\text{D2})$$

and Eq. (D1) can be solved analytically to yield

$$M_t = \begin{pmatrix} 1 & td_T(P_0)q_{\psi,0} & t/M & td_T(P_0)p_{\psi,0} \\ 0 & c_T(P_0) & td_T(P_0)p_{\psi,t} & s_T(P_0) \\ 0 & 0 & 1 & 0 \\ 0 & -s_T(P_0) & -td_T(P_0)q_{\psi,t} & c_T(P_0) \end{pmatrix} M_0, \quad (\text{D3})$$

where

$$c_T(P) := \cos[\hat{T}_{\text{nu+el}}(P)t/\hbar], \quad (\text{D4})$$

$$s_T(P) := \sin[\hat{T}_{\text{nu+el}}(P)t/\hbar], \quad (\text{D5})$$

and the propagation of quantum Darboux coordinates

$$q_{\psi,t} = c_T(P_0)q_{\psi,0} + s_T(P_0)p_{\psi,0}, \quad (\text{D6})$$

$$p_{\psi,t} = -s_T(P_0)q_{\psi,0} + c_T(P_0)p_{\psi,0} \quad (\text{D7})$$

for time t is equivalent to the standard propagation of electronic wavefunction $\psi_t = \exp[-it\hat{T}_{\text{nu+el}}(P_0)/\hbar]\psi_0$ since $\psi_t = (q_{\psi,t} + ip_{\psi,t})/\sqrt{2\hbar}$.

During the potential propagation, the equation of motion

$$\dot{M}_t = J^T \text{Hess}[\langle \hat{V}(Q_t) \rangle_{\psi_t}] M_t \quad (\text{D8})$$

for stability matrix M_t is obtained by reducing the effective Hamiltonian to $H_{\text{eff}}(x_{\text{eff}}) = \langle \hat{V}(Q) \rangle_{\psi}$ in Eq. (C6). The explicit form of the Hessian is

$$\text{Hess}[\langle \hat{V}(Q) \rangle_{\psi}] = \begin{pmatrix} \langle \text{Hess} \hat{V}(Q) \rangle_{\psi} & d_V(Q) q_{\psi} & 0 & d_V(Q) p_{\psi} \\ d_V(Q) q_{\psi} & \hat{V}(Q)/\hbar & 0 & 0 \\ 0 & 0 & 0 & 0 \\ d_V(Q) p_{\psi} & 0 & 0 & \hat{V}(Q)/\hbar \end{pmatrix}, \quad (\text{D9})$$

and Eq. (D8) can be solved analytically to yield

$$M_t = \begin{pmatrix} 1 & 0 & 0 & 0 \\ td_V(Q_0) p_{\psi,t} & c_V(Q_0) & 0 & s_V(Q_0) \\ -t \langle \text{Hess} \hat{V}(Q_0) \rangle_{\psi_0} & -td_V(Q_0) q_{\psi,0} & 1 & -td_V(Q_0) p_{\psi,0} \\ -td_V(Q_0) q_{\psi,t} & -s_V(Q_0) & 0 & c_V(Q_0) \end{pmatrix} M_0, \quad (\text{D10})$$

where

$$c_V(Q) := \cos[\hat{V}(Q)t/\hbar], \quad (\text{D11})$$

$$s_V(Q) := \sin[\hat{V}(Q)t/\hbar], \quad (\text{D12})$$

and the propagation of quantum Darboux coordinates

$$q_{\psi,t} = c_V(Q_0) q_{\psi,0} + s_V(Q_0) p_{\psi,0}, \quad (\text{D13})$$

$$p_{\psi,t} = -s_V(Q_0) q_{\psi,0} + c_V(Q_0) p_{\psi,0} \quad (\text{D14})$$

for time t is equivalent to the propagation of the electronic wavefunction $\psi_t = \exp[-it\hat{V}(Q_0)/\hbar]\psi_0$ since $\psi_t = (q_{\psi,t} + ip_{\psi,t})/\sqrt{2\hbar}$.

Supplementary material for: High-order geometric integrators for representation-free Ehrenfest dynamics

This document provides information supporting the main text. It contains the computational details (Sec. S1), efficiency of the high-order geometric integrators obtained using the triple-jump, Suzuki-fractal, and optimal composition schemes (Sec. S2), and detailed algorithms of the two and three time step methods (Sec. S3).

S1. COMPUTATIONAL DETAILS

In the exact quantum simulation, the full wavefunction Ψ_t was represented on a uniform four-dimensional grid that is a tensor product of two different two-dimensional grids for the nuclear and electronic degrees of freedom. A uniform grid of 101×101 points defined between $Q_n = -3$ a.u. and $Q_n = 3$ a.u. was used for the nuclear degrees of freedom. As for the electronic degrees of freedom, a uniform grid of 64×64 points defined between $q_n = -10$ a.u. and $q_n = 10$ a.u. was used; this grid was also used to represent the electronic wavefunction in Ehrenfest simulations. We employed the second-order VTV split-operator algorithm with time step $\Delta t = 0.1$ a.u. for the numerical propagation of Ψ_t .

To obtain the initial states, we solved the electronic time-independent Schrödinger equation [Eq. (53) of the main text] with the imaginary time propagation method:¹¹³ To prepare quantum initial state (51) of the main text, we solved the equation at every point on the nuclear grid. In contrast, to obtain the initial effective phase space point for Ehrenfest simulations [see Eq. (55) of the main text], we only had to solve the equation once at the initial nuclear position Q_0 .

S2. EFFICIENCY OF THE GEOMETRIC INTEGRATORS

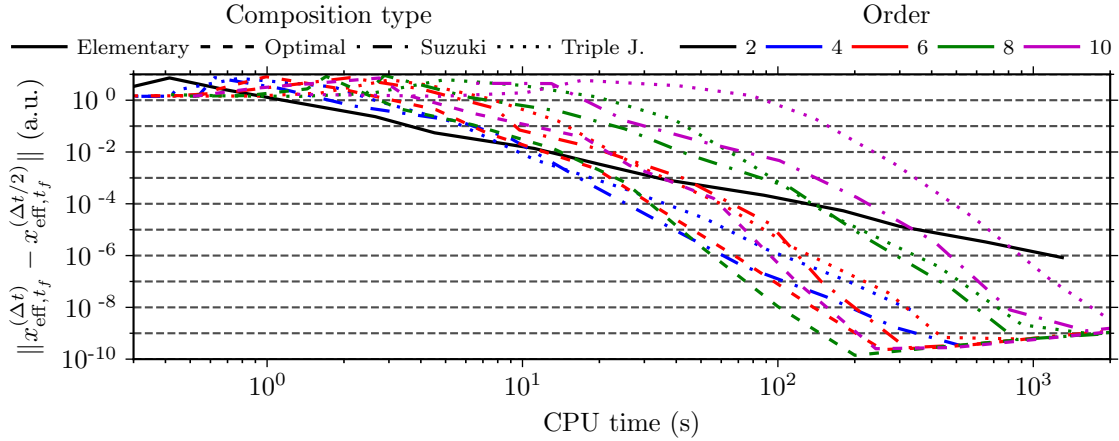


FIG. S1. Efficiency of the geometric integrators presented in Sec. IID of the main text. Like in the main text, efficiency is measured using the dependence of the convergence error on the computational cost (which we measure by CPU time). As expected, for each order of accuracy, the optimal composition scheme yields the most efficient method.

S3. DETAILED ALGORITHMS OF THE TWO AND THREE TIME STEP METHODS

A. Two time step method

The detailed algorithm of the two time step method is as follows (like in the main text, $\Delta t_{\text{el}} = \Delta t/n_{\text{el}}$):

(Verlet algorithm with time step Δt):

$$P_{t+\Delta t/2} = P_t - \frac{\Delta t}{2} \langle \hat{V}'(Q_t) \rangle_{\psi_t}$$

$$Q_{t+\Delta t} = Q_t + \Delta t M^{-1} \cdot P_{t+\Delta t/2}$$

$$P_{t+\Delta t} = P_{t+\Delta t/2} - \frac{\Delta t}{2} \langle \hat{V}'(Q_{t+\Delta t}) \rangle_{\psi_t}$$

Do $i = 1, \dots, n_{\text{el}}$

(VTV split-operator algorithm with time step Δt_{el}):

$$\psi_{t+i\Delta t_{\text{el}}} = \hat{U}_{\text{VTV}}^{(\Delta t_{\text{el}})}(Q_{t+\Delta t}, P_{t+\Delta t}) \psi_{t+(i-1)\Delta t_{\text{el}}}$$

End Do,

where the evolution operator

$$\hat{U}_{\text{VTV}}^{(\tau)}(Q, P) = \hat{U}_{\text{V}}^{(\tau/2)}(Q) \hat{U}_{\text{T}}^{(\tau)}(P) \hat{U}_{\text{V}}^{(\tau/2)}(Q) \quad (\text{S1})$$

for the VTV split-operator algorithm is composed of the potential and kinetic propagation steps,

$$\hat{U}_{\text{V}}^{(\tau)}(Q) = \exp[-i\tau\hat{V}(Q)/\hbar], \quad (\text{S2})$$

$$\hat{U}_{\text{T}}^{(\tau)}(P) = \exp[-i\tau\hat{T}_{\text{nu+el}}(P)/\hbar]; \quad (\text{S3})$$

here, $\hat{T}_{\text{nu+el}}(P) = T_{\text{nu}}(P) + \hat{T}_{\text{el}}$.

B. Three time step method

The detailed algorithm of the three time step method is as follows (like in the main text,

$\Delta t_{\text{nu-el}} = \Delta t/n_{\text{nu-el}} = \Delta t_{\text{el}}n_{\text{el}}/n_{\text{nu-el}}$):

(Propagation of nuclear momentum by $\Delta t/2$.)

$$P_{t+\Delta t/2} = P_t - \frac{\Delta t}{2} \langle \hat{V}'(Q_t) \rangle_{\psi_t}$$

Do $i = 1, \dots, n_{\text{nu-el}}$

(Propagation of nuclear position by $\Delta t_{\text{nu-el}}/2$.)

$$Q_{t+(2i-1)\Delta t_{\text{nu-el}}/2} = Q_{t+(i-1)\Delta t_{\text{nu-el}}} + \frac{\Delta t_{\text{nu-el}}}{2} M^{-1} \cdot P_{t+\Delta t/2}$$

Do $j = 1, \dots, n_{\text{el}}/n_{\text{nu-el}}$

(VTV split-operator algorithm with the time step of Δt_{el} .)

$$\psi_{t+(i-1)\Delta t_{\text{nu-el}}+j\Delta t_{\text{el}}} = \hat{U}_{\text{VTV}}^{(\Delta t_{\text{el}})}(Q_{t+(2i-1)\Delta t_{\text{nu-el}}/2}, P_{t+\Delta t/2}) \psi_{t+(i-1)\Delta t_{\text{nu-el}}+(j-1)\Delta t_{\text{el}}}$$

End Do

(Propagation of nuclear position by $\Delta t_{\text{nu-el}}/2$.)

$$Q_{t+i\Delta t_{\text{nu-el}}} = Q_{t+(2i-1)\Delta t_{\text{nu-el}}/2} + \frac{\Delta t_{\text{nu-el}}}{2} M^{-1} \cdot P_{t+\Delta t/2}$$

End Do

(Propagation of nuclear momentum by $\Delta t/2$.)

$$P_{t+\Delta t} = P_{t+\Delta t/2} - \frac{\Delta t}{2} \langle \hat{V}'(Q_{t+\Delta t}) \rangle_{\psi_{t+\Delta t}}.$$

REFERENCES

- ¹J. C. Tully and R. K. Preston, *J. Chem. Phys.* **55**, 562 (1971).
- ²J. C. Tully, *J. Chem. Phys.* **93**, 1061 (1990).
- ³J. R. Schmidt, P. V. Parandekar, and J. C. Tully, *J. Chem. Phys.* **129**, 044104 (2008).
- ⁴C. Lasser and T. Swart, *J. Chem. Phys.* **129**, 034302 (2008).
- ⁵J. E. Subotnik and N. Shenvi, *J. Chem. Phys.* **134**, 024105 (2011).
- ⁶G. D. Billing, *Chem. Phys. Lett.* **30**, 391 (1975).
- ⁷G. D. Billing, *J. Chem. Phys.* **64**, 908 (1976).
- ⁸J. C. Tully, *Faraday Discuss.* **110**, 407 (1998).
- ⁹D. A. Micha, *J. Chem. Phys.* **78**, 7138 (1983).
- ¹⁰S.-I. Sawada, A. Nitzan, and H. Metiu, *Phys. Rev. B* **32**, 851 (1985).
- ¹¹D. A. Micha and K. Runge, *Phys. Rev. A* **50**, 322 (1994).
- ¹²D. A. Micha, *J. Phys. Chem. A* **103**, 7562 (1999).
- ¹³X. Li, J. C. Tully, H. B. Schlegel, and M. J. Frisch, *J. Chem. Phys.* **123**, 084106 (2005).
- ¹⁴A. Bastida, J. Zúñiga, A. Requena, and B. Miguel, *J. Chem. Phys.* **129**, 154501 (2008).
- ¹⁵M. Vacher, D. Mendive-Tapia, M. J. Bearpark, and M. A. Robb, *Theor. Chem. Acc.* **133**, 1 (2014).
- ¹⁶A. Donoso and C. C. Martens, *J. Phys. Chem. A* **102**, 4291 (1998).
- ¹⁷R. Kapral and G. Ciccotti, *J. Chem. Phys.* **110**, 8919 (1999).
- ¹⁸Q. Shi and E. Geva, *J. Chem. Phys.* **121**, 3393 (2004).
- ¹⁹H.-D. Meyer and W. H. Miller, *J. Chem. Phys.* **70**, 3214 (1979).
- ²⁰G. Stock and M. Thoss, *Phys. Rev. Lett.* **78**, 578 (1997).
- ²¹W. H. Miller, *J. Phys. Chem. A* **113**, 1405 (2009).
- ²²S. J. Cotton, R. Liang, and W. H. Miller, *J. Chem. Phys.* **147**, 064112 (2017).
- ²³E. R. Dunkel, S. Bonella, and D. F. Coker, *J. Chem. Phys.* **129**, 114106 (2008).
- ²⁴N. Ananth and T. F. Miller, *J. Chem. Phys.* **133**, 234103 (2010).
- ²⁵T. J. H. Hele and N. Ananth, *Faraday Discuss.* **195**, 269 (2016).
- ²⁶W. Domcke and D. R. Yarkony, *Annu. Rev. Phys. Chem.* **63**, 325 (2012).
- ²⁷K. Takatsuka, T. Yonehara, K. Hanasaki, and Y. Arasaki, *Chemical Theory Beyond the Born-Oppenheimer Paradigm: Nonadiabatic Electronic and Nuclear Dynamics in Chemical Reactions* (World Scientific, Singapore, 2015).

- ²⁸M. P. Bircher, E. Liberatore, N. J. Browning, S. Brickel, C. Hofmann, A. Patoz, O. T. Unke, T. Zimmermann, M. Chergui, P. Hamm, U. Keller, M. Meuwly, H. J. Woerner, J. Vaníček, and U. Rothlisberger, *Struct. Dyn.* **4**, 061510 (2017).
- ²⁹T. Zimmermann and J. Vaníček, *J. Chem. Phys.* **132**, 241101 (2010).
- ³⁰T. Zimmermann and J. Vaníček, *J. Chem. Phys.* **136**, 094106 (2012).
- ³¹T. Zimmermann and J. Vaníček, *J. Chem. Phys.* **137**, 22A516 (2012).
- ³²P. V. Parandekar and J. C. Tully, *J. Chem. Theory Comput.* **2**, 229 (2006).
- ³³I. Loaiza and A. F. Izmaylov, *J. Chem. Phys.* **149**, 214101 (2018).
- ³⁴L. Blancafort, P. Hunt, and M. A. Robb, *J. Am. Chem. Soc.* **127**, 3391 (2005).
- ³⁵F. Wang, X. Xu, X. Hong, J. Wang, and B. Gou, *Phys. Lett. A* **375**, 3290 (2011).
- ³⁶W. Xie, S. Bai, L. Zhu, and Q. Shi, *J. Phys. Chem. A* **117**, 6196 (2013).
- ³⁷G. Li, B. Movaghar, A. Nitzan, and M. A. Ratner, *J. Chem. Phys.* **138**, 044112 (2013).
- ³⁸A. V. Akimov, R. Long, and O. V. Prezhdo, *J. Chem. Phys.* **140**, 194107 (2014).
- ³⁹Z. Kirson, R. Gerber, A. Nitzan, and M. Ratner, *Surface Science* **137**, 527 (1984).
- ⁴⁰Z. Kirson, R. Gerber, A. Nitzan, and M. Ratner, *Surface Science* **151**, 531 (1985).
- ⁴¹M. Head-Gordon and J. C. Tully, *J. Chem. Phys.* **103**, 10137 (1995).
- ⁴²I. G. Ryabinkin and A. F. Izmaylov, *J. Phys. Chem. Lett.* **8**, 440 (2017).
- ⁴³M. S. Topaler, T. C. Allison, D. W. Schwenke, and D. G. Truhlar, *J. Chem. Phys.* **109**, 3321 (1998).
- ⁴⁴S. Klein, M. J. Bearpark, B. R. Smith, M. A. Robb, M. Olivucci, and F. Bernardi, *Chem. Phys. Lett.* **292**, 259 (1998).
- ⁴⁵R. Gherib, I. G. Ryabinkin, and A. F. Izmaylov, *J. Chem. Theory Comput.* **11**, 1375 (2015).
- ⁴⁶A. Kelly, N. Brackbill, and T. E. Markland, *J. Chem. Phys.* **142**, 094110 (2015).
- ⁴⁷T. Zimmermann and J. Vaníček, *J. Chem. Phys.* **141**, 134102 (2014).
- ⁴⁸N. Ananth, C. Venkataraman, and W. H. Miller, *J. Chem. Phys.* **127**, 084114 (2007).
- ⁴⁹D. V. Shalashilin, *J. Chem. Phys.* **130**, 244101 (2009).
- ⁵⁰T. Ma, M. Bonfanti, P. Eisenbrandt, R. Martinazzo, and I. Burghardt, *J. Chem. Phys.* **149**, 244107 (2018).
- ⁵¹L. Chen, K. Sun, D. V. Shalashilin, M. F. Gelin, and Y. Zhao, *J. Chem. Phys.* **154**, 054105 (2021).
- ⁵²F. A. Bornemann, P. Nettesheim, and C. Schütte, *J. Chem. Phys.* **105**, 1074 (1996).

- ⁵³E. Q. Feng, D. A. Micha, and K. Runge, *Int. J. Quant. Chem.* **40**, 545 (1991).
- ⁵⁴F. Ding, J. J. Goings, H. Liu, D. B. Lingerfelt, and X. Li, *J. Chem. Phys.* **143**, 114105 (2015).
- ⁵⁵E. Hairer, C. Lubich, and G. Wanner, *Geometric Numerical Integration: Structure-Preserving Algorithms for Ordinary Differential Equations* (Springer Berlin Heidelberg New York, 2006).
- ⁵⁶B. Leimkuhler and S. Reich, *Simulating Hamiltonian Dynamics* (Cambridge University Press, 2004).
- ⁵⁷C. Lubich, *From Quantum to Classical Molecular Dynamics: Reduced Models and Numerical Analysis*, 12th ed. (European Mathematical Society, Zürich, 2008).
- ⁵⁸P. Nettesheim, F. A. Bornemann, B. Schmidt, and C. Schütte, *Chemical Physics Letters* **256**, 581 (1996).
- ⁵⁹G. Strang, *SIAM J. Num. Analysis* **5**, 506 (1968).
- ⁶⁰R. I. McLachlan and G. R. W. Quispel, *Acta Numerica* **11**, 341 (2002).
- ⁶¹M. D. Feit, J. A. Fleck, Jr., and A. Steiger, *J. Comp. Phys.* **47**, 412 (1982).
- ⁶²L. Verlet, *Phys. Rev.* **159**, 98 (1967).
- ⁶³D. Fang, S. Jin, and C. Sparber, *Multiscale Model. Simul.* **16**, 900 (2018).
- ⁶⁴A. Kelly, R. van Zon, J. Schofield, and R. Kapral, *J. Chem. Phys.* **136**, 084101 (2012).
- ⁶⁵J. O. Richardson, P. Meyer, M.-O. Pleinert, and M. Thoss, *Chem. Phys.* **482**, 124 (2017).
- ⁶⁶M. S. Church, T. J. H. Hele, G. S. Ezra, and N. Ananth, *J. Chem. Phys.* **148**, 102326 (2018).
- ⁶⁷J. E. Runeson and J. O. Richardson, *J. Chem. Phys.* **152**, 084110 (2020).
- ⁶⁸J. J. Goings, P. J. Lestrangle, and X. Li, *Wiley Interdiscip. Rev. Comput. Mol. Sci.* **8**, e1341 (2018).
- ⁶⁹X. Li, N. Govind, C. Isborn, A. E. DePrince, and K. Lopata, *Chem. Rev.* **120**, 9951 (2020).
- ⁷⁰H. Yoshida, *Phys. Lett. A* **150**, 262 (1990).
- ⁷¹M. Suzuki, *Phys. Lett. A* **146**, 319 (1990).
- ⁷²R. I. McLachlan, *SIAM J. Sci. Comp.* **16**, 151 (1995).
- ⁷³W. Kahan and R.-C. Li, *Math. Comput.* **66**, 1089 (1997).
- ⁷⁴M. Sofroniou and G. Spaletta, *Optim. Method Softw.* **20**, 597 (2005).
- ⁷⁵K. Hader, J. Albert, E. K. U. Gross, and V. Engel, *J. Chem. Phys.* **146**, 074304 (2017).

- ⁷⁶J. Albert, K. Hader, and V. Engel, *J. Chem. Phys.* **147**, 064302 (2017).
- ⁷⁷T. Schaupp and V. Engel, *J. Chem. Phys.* **151**, 084309 (2019).
- ⁷⁸S. Shin and H. Metiu, *J. Chem. Phys.* **102**, 9285 (1995).
- ⁷⁹S. Shin and H. Metiu, *J. Phys. C* **100**, 7867 (1996).
- ⁸⁰E. J. Heller, *J. Chem. Phys.* **64**, 63 (1976).
- ⁸¹R. B. Gerber, V. Buch, and M. A. Ratner, *J. Chem. Phys.* **77**, 3022 (1982).
- ⁸²R. Gerber, M. Ratner, and V. Buch, *Chem. Phys. Lett.* **91**, 173 (1982).
- ⁸³R. H. Bisseling, R. Kosloff, R. B. Gerber, M. A. Ratner, L. Gibson, and C. Cerjan, *J. Chem. Phys.* **87**, 2760 (1987).
- ⁸⁴M. Messina and R. D. Coalson, *J. Chem. Phys.* **90**, 4015 (1989).
- ⁸⁵P. A. M. Dirac, *Math. Proc. Camb. Phil. Soc.* **26**, 376–385 (1930).
- ⁸⁶J. Frenkel, *Wave mechanics* (Clarendon Press, Oxford, 1934).
- ⁸⁷J. E. Marsden and T. S. Ratiu, *Introduction to mechanics and symmetry: a basic exposition of classical mechanical systems*, Vol. 17 (Springer Science & Business Media, 1999).
- ⁸⁸T. Ohsawa and M. Leok, *J. Phys. A* **46**, 405201 (2013).
- ⁸⁹R. Abraham and J. E. Marsden, *Foundations of mechanics* (Addison-Wesley Publishing Company, Inc., 1978).
- ⁹⁰M. Wehrle, M. Šulc, and J. Vaníček, *Chimia* **65**, 334 (2011).
- ⁹¹J. Roulet, S. Choi, and J. Vaníček, *J. Chem. Phys.* **150**, 204113 (2019).
- ⁹²S. Choi and J. Vaníček, *J. Chem. Phys.* **151**, 234102 (2019).
- ⁹³S. Choi and J. Vaníček, *J. Chem. Phys.* **150**, 204112 (2019).
- ⁹⁴H. Nakamura, *Nonadiabatic Transition: Concepts, Basic Theories and Applications*, 2nd ed. (World Scientific Publishing Company, 2012).
- ⁹⁵S. Mukamel, *Principles of nonlinear optical spectroscopy*, 1st ed. (Oxford University Press, New York, 1999).
- ⁹⁶W. Domcke, D. Yarkony, and H. Köppel, *Conical intersections: electronic structure, dynamics & spectroscopy*, Vol. 15 (World Scientific, 2004).
- ⁹⁷E. J. Heller, *The semiclassical way to dynamics and spectroscopy* (Princeton University Press, Princeton, NJ, 2018).
- ⁹⁸X. Li, S. M. Smith, A. N. Markevitch, D. A. Romanov, R. J. Levis, and H. B. Schlegel, *Phys. Chem. Chem. Phys.* **7**, 233 (2005).

- ⁹⁹J. Theilhaber, Phys. Rev. B **46**, 12990 (1992).
- ¹⁰⁰K. Yabana and G. F. Bertsch, Phys. Rev. B **54**, 4484 (1996).
- ¹⁰¹A. Castro, M. A. Marques, J. A. Alonso, G. F. Bertsch, and A. Rubio, Eur. Phys. J. D **28**, 211 (2004).
- ¹⁰²C. M. Isborn, X. Li, and J. C. Tully, J. Chem. Phys. **126**, 134307 (2007).
- ¹⁰³Y. Miyamoto, A. Rubio, and D. Tománek, Phys. Rev. Lett. **97**, 126104 (2006).
- ¹⁰⁴S. Meng and E. Kaxiras, J. Chem. Phys. **129**, 054110 (2008).
- ¹⁰⁵X. Andrade, A. Castro, D. Zueco, J. L. Alonso, P. Echenique, F. Falseto, and Á. Rubio, J. Chem. Theory Comput. **5**, 728 (2009).
- ¹⁰⁶W. Liang, C. M. Isborn, A. Lindsay, X. Li, S. M. Smith, and R. J. Levis, J. Phys. Chem. A **114**, 6201 (2010).
- ¹⁰⁷A. Castro, M. A. L. Marques, and A. Rubio, J. Chem. Phys. **121**, 3425 (2004).
- ¹⁰⁸M. A. L. Marques and E. K. U. Gross, “Time-dependent density functional theory,” in *Primer in Density Functional Theory*, edited by C. Fiolhais, F. Nogueira, and M. A. L. Marques (Springer Berlin Heidelberg, Berlin, Heidelberg, 2003) pp. 144–184.
- ¹⁰⁹M. A. Marques, A. Castro, G. F. Bertsch, and A. Rubio, Comput. Phys. Commun **151**, 60 (2003).
- ¹¹⁰X. Andrade, J. Alberdi-Rodriguez, D. A. Strubbe, M. J. T. Oliveira, F. Nogueira, A. Castro, J. Muguerza, A. Arruabarrena, S. G. Louie, A. Aspuru-Guzik, A. Rubio, and M. A. L. Marques, J. Phys.: Cond. Matt. **24**, 233202 (2012).
- ¹¹¹N. Tancogne-Dejean, M. J. T. Oliveira, X. Andrade, H. Appel, C. H. Borca, G. Le Breton, F. Buchholz, A. Castro, S. Corni, A. A. Correa, U. De Giovannini, A. Delgado, F. G. Eich, J. Flick, G. Gil, A. Gomez, N. Helbig, H. Hübener, R. Jestädt, J. Jornet-Somoza, A. H. Larsen, I. V. Lebedeva, M. Lüders, M. A. L. Marques, S. T. Ohlmann, S. Pipolo, M. Rampp, C. A. Rozzi, D. A. Strubbe, S. A. Sato, C. Schäfer, I. Theophilou, A. Welden, and A. Rubio, J. Chem. Phys. **152**, 124119 (2020).
- ¹¹²J. M. Lee, *Manifolds and Differential Geometry*, Vol. 107 (American Mathematical Soc., 2009).
- ¹¹³R. Kosloff and H. Tal-Ezer, Chem. Phys. Lett. **127**, 223 (1986).